Neoproterozoic ice sheets and olistoliths

Le Heron, Daniel P.; Busfield, Marie E.; Prave, Anthony R.

Published in:
Journal of the Geological Society

DOI:
10.1144/jgs2013-130

Publication date:
2014

Citation for published version (APA):
Le Heron, D. P., Busfield, M. E., & Prave, A. R. (2014). Neoproterozoic ice sheets and olistoliths: Multiple glacial cycles in the Kingston Peak Formation, California. *Journal of the Geological Society*, *171*(4), 525-538. https://doi.org/10.1144/jgs2013-130

Neoproterozoic ice sheets and olistoliths: multiple glacial cycles in the Kingston Peak Formation, California

DANIEL P. LE HERON[*], MARIE E. BUSFIELD[*], ANTHONY R. PRAVE[†]

[*] *Department of Earth Sciences, Queen's Building, Royal Holloway University of London, Egham, Surrey, TW20 0BY, UK (E-mail: daniel.le-heron@rhul.ac.uk)*

[†] *Department of Earth and Environmental Sciences, University of St Andrews, St Andrews, KY16 9AL, UK*

Abstract: The Kingston Peak Formation is a diamictite-bearing succession that crops out in the Death Valley region, California, USA. An exceptionally thick (>1.5 km) outcrop belt in its type area (the Kingston Range), provides clear insights into the dynamics of mid-Cryogenian ('Sturtian') ice sheets in Laurentia. Seven detailed logs allow the lateral and vertical distribution of facies associations to be assessed. We recognise (1) diamictite facies association (ice-proximal glacigenic debris flows), (2) lonestone-bearing facies association (ice-marginal hemipelagic deposits and low-density gravity flows with ice-berg rafting), (3) pebble to boulder conglomerate facies association (ice-proximal co-genetic glacigenic debris flows and high-density turbidites), (4) megaclast facies association (olistostrome and hemipelagic sediments subject to ice-rafting), and (5) interbedded heterolithics facies association (low-density turbidites and hemipelagic deposits). The stratigraphic motif allows three glacial cycles to be inferred across the range. Ice-minimum conditions interrupting the Kingston Peak are associated with the development of an olistostrome complex, succeeded by a thick accumulation of boulder conglomerates deposited during ice re-advance. The data testify to a strong glacial influence on sedimentation within this ancient subaqueous succession, and to highly dynamic ice sheet behaviour with clear glacial cycles during the Sturtian glaciation.

The snowball Earth hypothesis (Hoffman et al., 1998) postulates that pan-global ice sheets covered the Earth's surface at multiple intervals in the Cryogenian (850-635 Ma), traditionally correlated to an older 'Sturtian' and younger 'Marinoan' glaciation. Evidence for a "hard" snowball Earth has become difficult to support in recent years, as evidence has emerged of highly dynamic ice sheets, including evidence for open water (e.g. Leather et al., 2002; Arnaud, 2004; Allen and Etienne, 2008; Le Heron et al., 2011). The extent to which Neoproterozoic ice sheets mirrored the behaviour of their Phanerozoic counterparts has remained hotly debated (Etienne et al., 2007). However, detailed study of the sedimentary architecture of many Cryogenian glacial successions is long overdue. Such studies provide insight into Earth surface environments during the Cryogenian, shedding light on the scale and intensity of glacial cycles, and, importantly, the link between the break-up of the Rodinia supercontinent and glaciation (Eyles and Januszczak, 2004).

Whilst the task is important, determining the dimensions and behavioural characteristics of Neoproterozoic ice sheets is challenging. The snowball Earth hypothesis (Hoffman et al., 1998) requires globally extensive ice, yet the location of ice sheet grounding lines remains poorly defined. In the Death Valley region, California, the 'Sturtian'-equivalent Kingston Peak Formation is commonly interpreted as the product of glaciomarine deposition beyond the grounded ice margin (Hazzard, 1939; Wright et al., 1974; Miller, 1985; Mrofka and Kennedy, 2012), although a solely glacial derivation is not accepted by all (e.g. Troxel 1982). Outcrop belts have been tectonically dismembered by Tertiary extensional deformation but individual fault blocks can be reconstructed to reveal laterally and vertically variable lithofacies assemblages comprising strata that include several kilometres of turbidites, diamictites of mass-flow affinity and boulder-size lonestones (Troxel 1982; Miller

1985, 1987; Prave, 1999; Mrofka and & Kennedy, 2011), many interpreted as dropstones (Abolins et al., 2000; Corsetti and Kaufman, 2003).

This paper provides a thorough sedimentological analysis of the Kingston Peak Formation in its type area, the Kingston Range (**Fig. 1**), and includes detailed descriptions of facies and facies associations, documents their distribution in map view, and presents a glacial depositional model for their accumulation. In doing so we propose three glacial cycles within the mid-Cryogenian succession, and offer a refined interpretation for the origin of km-scale megaclasts. This study therefore provides a stratigraphic framework to facilitate comparison with other 'Sturtian' sequences elsewhere in the Cordillera.

Study area and lithostratigraphy

The Kingston Range exposes a superb outcrop belt of the Kingston Peak Formation, a 300-2400 m thick heterolithic, predominantly siliciclastic succession preserving a record of Cryogenian glaciation (**Fig. 1**). The Kingston Peak Formation overlies microbial carbonates of the Beck Spring Dolomite and is truncated by the Noonday Dolomite (**Fig. 1**). Following on from the mapping of Wright and Troxel and their colleagues (as synthesised on the United States Geological Survey Open File Report P124-000412), Prave (1999) applied a fourfold subdivision of the Kingston Peak Formation, with units termed KP1-KP4. KP1 is now known to be genetically unrelated to the glaciogenic portion of the Kingston Peak Formation (Prave, 1999; Macdonald et al., 2013), and is thus excluded from this study. Units KP2 and KP3 account for almost all the remaining stratigraphy in the Kingston Peak Formation across the southern Death Valley region and the Kingston Range (Macdonald et al., 2103), with only thin, patchy development of the fourth unit termed KP4. Units KP2 and KP3 are tentatively assigned to an older Cryogenian ('Sturtian') glaciation, and KP4 is attributed to the younger Cryogenian ('Marinoan') glaciation (Prave, 1999; Petterson et al., 2011a,b; Macdonald et al.,

2013), with an interglacial stratigraphy well developed in the Panamint Range (Miller, 1985; Petterson et al., 2011b). Whilst absolute age dates are lacking, carbon isotope stratigraphy of the overlying Noonday Dolomite compares closely to basal Ediacaran cap carbonates worldwide, dated at 635 Ma (Kennedy et al., 1998; Prave, 1999; Corsetti and Kaufmann, 2003; Petterson et al., 2011a,b; Macdonald et al., 2013), and the work of Petterson et al. (2011a,b) supports strongly the inference that it is the younger Cryogenian (Marinoan) cap. Other stratigraphies have been proposed but these are variations on the overall framework noted above. For example, Mrofka (2010) proposes subdividing the Kingston Peak Formation into, from the base up, the Saratoga Hills Sandstone (KP1), the Alexander Hills Diamictite (KP2), the Silver Rule Mine Member (basal KP3) and the Jupiter Mine Member (upper KP3). Macdonald et al. (2013) highlight the likely linkages between the Death Valley succession and those elsewhere in western Laurentia and define four inter-regionally developed, unconformity-bound tectonostratigraphic units (TU1-4) as a means of establishing a craton-margin stratigraphic framework. The present paper deals almost exclusively with rocks contained within units KP2 and KP3, which are components of TU3a and TU3b of Macdonald et al. (2013).

In the vicinity of section 3 at Horsethief Spring (**Fig. 1**), the outcrop belt is cut by a series of en-echelon, NE-SW trending faults. Some of these faults were active during sedimentation, evidenced by the abrupt termination of some facies against them, as well as thickness increases of others across them. They are interpreted as an array of normal faults that essentially partitioned the basin into horst-graben structures (**Fig. 1**, section 3) superimposed on the regional southward dipping palaeoslope. Studied sections were carefully examined away from these fault surfaces in order to avoid stratigraphic repetition and fault-related deformation.

Facies analysis

The high degree of lateral and vertical continuity of strata across the Kingston Range enables detailed lithofacies analysis. Five lithofacies associations (**Fig. 1**) are distinguished: (i) diamictite, (ii) lonestone-bearing, (iii) megaclast, (iv) pebble to boulder conglomerate, and (v) interbedded heterolithics facies associations. The following descriptions cross-reference the correlation panel (**Fig. 2**).

Diamictite facies association: description

These deposits encompass sandy and silty, grey, buff-weathering diamictites, with a range of clast-rich to clast-poor varieties recorded. The diamictite facies association occurs at two stratigraphic levels in the Kingston Range (**Fig. 2**), locally with uninterrupted stratigraphic thicknesses of up to 65 m (section 5). At the outcrop scale, clear intercalation of carbonate-matrix diamictites with siliciclastic-matrix diamictites is observed (e.g. section 1, **Fig. 2**; **Fig. 3A**). Clast lithologies include massive and laminated dolostone (Crystal Spring Formation and Beck Spring Dolomite), schist, leucogranite, siltstone (basal Kingston Peak), quartzite, and chloritized diabase. Striated clasts (**Fig. 3B**) are common.

Interbedded silty, stratified diamictites and sandy, massive diamictites are recognised locally at the metre-scale (e.g. section 2, 180-200 m, **Fig. 2**). The former are typically ungraded and tend towards more clast-poor varieties, but in places preserve lonestones with impact related deformation structures (**Fig. 3C**). Finer-grained intervals show intercalations of granular and clast-free siltstone layers on the cm-scale, where isolated examples of mm- to cm-scale rootless folds and sheared boudins also occur (**Fig. 3D**). Massive diamictites (**Fig. 3E**) are also commonly ungraded, with local evidence of increased clast abundance upsection within individual beds. Such intervals also include cut-and-fill geometries, with 2-3 m wide incisions, filled with sandy, massive diamictite truncating silty, stratified varieties (e.g.

123 section 2, 203 m, **Fig. 2**). Rarely, discrete, erosively-based sandstone lenses interrupt massive
124 diamictites (e.g. section 1, 139 m, **Fig. 2**). Micromorphological investigation reveals
125 comparatively clast-rich and clast-poor stratified diamictites (**Fig. 3F**), intercalated with 1-2
126 mm thick graded beds. This approach also reveals normal faults with millimetre-scale throws,
127 flame structures, rotated intraclasts, and the effects of loading or differential compaction
128 beneath clast-rich diamictites (**Fig. 3F**).

129

130 *Diamictite facies association: interpretation*

131 Macdonald et al. (2013) described unit KP2 as a "massive diamictite" and unit KP3 as a
132 stratified diamictite, but we emphasise that only those strata of our diamictite facies
133 association (unit KP2) can texturally be described as diamictite (Moncrieff, 1989; Hambrey
134 and Glasser, 2003). The massive diamictite lithofacies in this study are interpreted as a series
135 of glacigenic debris flows (GDFs) derived via downslope re-working of inherently unstable
136 sediment delivered to the ice-grounding line (e.g. Elverhøi et al., 2002,Ó Cofaigh et al. 2002,
137 Benn and Evans, 2010). Beds which exhibit inverse grading are interpreted to result from a
138 combination of kinetic sieving and upward clast migration: common processes during
139 laminar sediment remobilisation (Bagnold, 1954; Talling et al., 2012). Erosive contacts and
140 cut-and-fill structures are interpreted to record cannibalisation of underlying sediments during
141 repeated sediment gravity flow emplacement. Conversely, the predominance of planar, non-
142 erosive contacts is attributed to hydroplaning during flow emplacement, whereby elevated
143 fluid contents both lubricate and sustain the flow, and simultaneously protect the underlying
144 bed from cannibalisation (e.g. Laberg and Vorren, 2000). This process also enables greater
145 run-out distances, which may contribute to the absence of subglacial or ice-contact
146 deformation features. Both stratified and massive diamictites are thought to accumulate

147 within the ice-proximal zone, as more distally they would likely undergo flow transformation
148 to more dilute, co-genetic turbidity flows (Hampton, 1972; Talling et al., 2012). This is
149 consistent with the preservation of clast striations, which would be expected to be removed
150 during clast-on-clast abrasion under prolonged sediment re-working.

151 Isolated lonestones with impact-related deformation structures are interpreted as ice-
152 berg rafted debris, wherein debris-laden icebergs are released from the ice front, leading to
153 rain-out in the ice-proximal zone as the basal debris layer melts. The diverse size and
154 lithology of ice-rafted clasts is considered more characteristic of ice-berg than ice-shelf
155 rafting (Pudsey et al., 2006; Reinardy et al., 2009; Domack and Hoffman, 2011), wherein
156 freeze-on of the basal debris layer would also inhibit widespread rain-out (e.g. Anderson et
157 al. 1991; Hambrey and Glasser, 2012). In addition, sub-ice shelf diamicton facies are
158 reportedly characterised by numerous intraformational sediment clasts derived through
159 subglacial deformation near the grounding line ("till pellets": e.g. Domack and Harris, 1998;
160 Khatwa and Tulaczyk, 2001; Evans and Pudsey, 2002), which are absent from the diamictite
161 facies association described herein.

162 At the outcrop scale, the presence of rootless folds and sheared boudins might be
163 argued to indicate sediment shearing, either in response to ice-sheet grounding (Arnaud, 2012
164 and refs therein), or potentially a shearing basal layer in a debris flow (Phillips, 2006). At the
165 thin section scale, the primary source of the stratification is clearly sedimentary, rather than
166 of shear origin, with intercalated clast-rich and clast-poor diamictites on the lamina scale, and
167 graded sandstone laminae. The suite of deformation features (flame structures, load
168 structures, extensional microfaults) is more suggestive of post-depositional loading in concert
169 with local fluid escape. None of the rotational structures characteristic of Sturtian
170 glacitectonites in northern Namibia (Busfield and Le Heron, 2013) were observed in the
171 Kingston Range sections.

Lonestone-bearing facies association: description

These deposits are typically thin, ranging in thickness from 12 m (section 5, **Fig. 2**) to 27 m (section 1, **Fig. 2**). The dominant lithology is well-stratified grey siltstone and shale, punctuated by 10-20 cm thick sandstone beds, 5-40 cm thick pebbly conglomerate layers, and massive, silty diamictites. The siltstone and shale intervals are well laminated throughout, with isolated examples of current ripple cross-lamination. These intervals bear lonestones, typically of pebble to cobble size, of dolostone, siltstone, quartzite, and rarely chloritised metabasite. In places, clasts occur as bedding-parallel trains of pebbles and cobbles (**Fig. 4A**), but more commonly as outsized clasts (lonestones) (**Fig. 4B**). The lonestones typically puncture underlying laminae; overlying laminae are undeformed, draping the lonestones (**Fig. 4C**).

Lonestone-bearing facies association: Interpretation

The well stratified siltstones and shales are interpreted as hemipelagic deposits, largely derived from fine-grained sediment plumes triggered by associated silt and sand underflows. The latter, including the thick sandstone interbeds and ripple cross-laminated siltstones, are interpreted as the product of dilute, low-density turbidity currents (Bouma T_{c-e}: e.g. Talling et al., 2012), where fully turbulent conditions are required for ripple development (Baas et al., 2011).Thin beds of massive diamictite are interpreted as glacigenic debris flow deposits, in a similar manner to their thicker counterparts in the diamictite facies association. Lonestones with clear impact structures indicate ice-rafting, with the diversity of clast lithologies indicative of iceberg as opposed to ice-shelf rafted debris (Pudsey et al., 2006; Reinardy et al., 2009; Domack and Hoffman, 2011). The finer grained nature of the host sediments, and greater abundance of dilute turbidites than their less evolved co-genetic debrites supports

196 accumulation in an ice-marginal setting, by comparison to the ice-proximal setting of the
197 diamictite facies association.

198

199 *Pebble to boulder-conglomerate facies association: description*

200 These deposits are dominated by clast- and matrix-supported conglomerates with a sandy
201 matrix, with uninterrupted stratigraphic thicknesses that can be as much as > 250m (e.g.
202 section 7, **Fig. 2**). The total thickness of the facies association is highly variable across the
203 range, not exceeding 40 m at section 3 (**Fig. 2**). Maximum clast size is typically cobble to
204 boulder dimensions (**Fig. 5A**); we differentiate these from pebbly conglomerates in our
205 logged sections (**Fig. 2**). Clasts are typically equant to irregular, ranging from angular to
206 rounded, with sub-rounded clasts predominant. Compositionally, clasts are dominated by
207 dolostones derived from the Beck Spring Dolomite, including microbial laminites and
208 crystalline dolostone, with sandstone clasts also common. Bed thicknesses range from ~20
209 cm to >10 m. Bed contacts are typically diffuse wherein normally graded, finer-grained beds
210 pass vertically into massive, ungraded boulder conglomerates (e.g. section 7, 175 m, **Fig. 2**).
211 In the same section, both fining- and coarsening-upward motifs are apparent, and are
212 partitioned by clast-poor sandstone (**Fig. 5B**); otherwise, many beds are structureless at the
213 base, passing upwards into plane-bedded gravels (e.g. section 7, 233 m: **Fig. 2**). Trough
214 cross-strata are also locally developed at the metre-scale, both within pebble-conglomerates
215 and intercalated coarse-grained sandstones (**Fig 5C**). On the decametre scale, thick packages
216 dominated by stratified, pebbly conglomerates (**Fig 2**, section 2, 320-350 m) alternate with
217 cobble and boulder-dominated units (**Fig. 2**, section 2, 350-415 m; **Fig. 5D**).

218

Pebble to boulder conglomerate facies association: interpretation

This facies association is interpreted as the product of glaciogenic debris flows and associated high-density turbidites. Limited palaeocurrent data from cross strata and cross laminae supports southward dipping palaeoslopes. The considerable uninterrupted thickness (>250 m in individual sections) testifies to a sustained interval of high sediment influx. The clear differentiation into predominantly cobble- to boulder-bearing beds and pebbly beds implies variations in energy levels or sediment supply, interpreted as the product of pulsed sediment delivery from the ice-grounding line. In this setting, high rates of sedimentation promote instability and repeated slope failure (e.g. Vorren et al., 1998; Dimakis et al., 2000; Benn and Evans, 2010), triggering downslope sediment remobilisation. The coarsening upward, structureless beds are interpreted as debrites, reflecting processes of upward clast migration and kinetic sieving (e.g. Talling et al., 2012), as recorded in the diamictite facies association. The clast angularity may imply a short transport interval, although the predominance of sub-rounded clasts underscores the importance of intra-flow clast abrasion. The fining-upwards conglomerates are interpreted as co-genetic high-density turbidites (Hampton, 1972; Talling et al., 2012). This is supported by the overall absence of bedforms, hindered by both rapid deposition and dampening of turbulence under high sediment concentrations (Talling et al., 2012). Both outcrop (Amy and Talling, 2006) and experimental approaches increasingly emphasise the co-genetic (bipartite: Tinterri et al., 2003) link between turbidity flows and debris flows. This process frequently occurs through transformation of moderate strength debris flows into more dilute ('linked') turbulent flows during mixing with the overlying water body (Talling et al., 2012), and commonly occurs within ice-proximal zones under high sedimentation rates (Benn & Evans, 2010). This setting is further supported by the occurrence of striated pebbles, reported by Macdonald et al. (2013) and Mrofka and Kennedy (2011), which would be unlikely to survive significant re-working and clast abrasion beyond

244 the ice-proximal zone. The co-genetic nature of debrites and turbidites may also account for
245 the diffuse boundaries between beds.

246 The association of debrites and turbidites is strong evidence that they were deposited
247 in a marine setting. Thus, earlier interpretations of these strata as "terrestrial fanglomerates"
248 are rejected (Mrofka, 2010; Mrofka and Kennedy, 2011). It is recognised that high
249 concentrations of boulder-bearing gravels could be produced by terrestrial jökulhlaup
250 outbursts onto sandur plains, associated with catastrophic release of turbulent meltwater
251 (Marren et al., 2009). However, these are typically marked by a suite of sedimentary
252 structures such as metre-scale antidunes and megaripples, even in gravels, as a result of
253 sustained flow over several hours or more (Duller et al., 2008). These characteristics are
254 lacking in the pebble to boulder conglomerate facies association. Moreover, features
255 characterising subaerial exposure such as palaeosols (Sheldon and Tabor, 2009), desiccation
256 cracks or aeolian deflation surfaces are lacking.

257

258 *Megaclast facies association: description*

259 This facies association consists of metre- to hundreds-of-metre-scale blocks (megaclasts) that
260 occur at a number of levels over a ~1000 m interval. The scale of the blocks is amply
261 demonstrated in panoramic view (**Fig, 6A, B**), and the facies association is particularly well
262 expressed in section 5 (**Fig. 2**). First described by Troxel (1966), the blocks are tabular
263 bodies with highly irregular edges (**Fig. 2, Fig. 6A**, **B**); most are carbonate lithologies derived
264 from the Crystal Spring Formation and Beck Spring Dolomite, but also comprise arkosic
265 sandstones and granular conglomerates (**Fig. 2**, section 5, 180-190 m), intensely sheared,
266 carbonate-dominated diamictite beds (**Fig. 2**, section 5, 157 m; **Fig. 6C**) and gneissic
267 basement. Internally they commonly comprise coherent beds, some of which are

stratigraphically inverted (i.e. upside down; Macdonald et al. 2013). Between the blocks, exposure is often poor. In places, however, well-stratified shales are preserved in continuous sections more than 10 m thick (**Fig. 2**) which onlap individual dolostone megaclasts **(Fig. 6D**).

Megaclast facies association: interpretation

The megaclast facies association is interpreted as an olistostrome (also see Macdonald et al., 2013), with the blocks representing constituent olistoliths and the interstitial shale representing background sedimentation. The planform distribution of the blocks (**Fig. 1**) demonstrates that whereas their strike is approximately bedding-parallel, each is an isolated fragment. Their size and angularity implies a short transport distance, and their source has been proposed to lie a few kilometres to the north of the outcrop belt (Macdonald et al., 2013). The presence of stratigraphically inverted olistoliths supports deposition via downlope gravity sliding (Robertson, 1977) and toppling, rather than debris flow slumping (Heck and Speed, 1987; Wendorff, 2005).

The onlap relationship of the shales against the olistoliths demonstrates that they represent background sedimentation prior to, during, and following olistolith emplacement. Comparable hemipelagic intervals have been encountered in other olistostromes (Heck and Speed, 1987). Isolated lonestones within the shale facies are interpreted as ice-rafted debris, suggesting deposition of the olistostrome concurrent with disintegration of the ice front. This process would be expected to destabilise a marine-terminating ice mass, thereby providing a plausible mechanism for inducing catastrophic slope failure. Under this scenario, icebergs may be calved from the ice front, releasing debris into the interstitial shales. An alternative explanation is that the megaclasts are themselves ice-rafted, but the absence of impact-related

deformation features within the underlying shales, the sheer scale of the megaclasts, and the evidence for inversion during downslope movement are considered incompatible with this scenario.

It has long been recognised that syn-depositional extensional tectonism occurred concomitant with sedimentation (e.g. Prave, 1999, and references therein), and is considered to be a key factor in formation of the olistostrome (e.g. Macdonald et al., 2013, and references therein). In light of the evidence for ice-rafting accompanying accumulation of the olistoliths, the role of glaciation in triggering their remobilisation can be invoked. Prior to deposition, ice cover in the source area of the megaclasts may have contributed to break-up of the bedrock through processes of freeze-thaw, whereby the exploitation of joints by meltwater and permafrost development resulted in *in situ* fracturing. With the overburden of the ice cover, the fractured bedrock would be held in place as tabular blocks. As ice retreated, unloading accompanied by isostatic rebound de-stabilised the fractured substrate. Therefore, the combined influence of removal of the ice buttress and syn-sedimentary tectonism, potentially during isostatic rebound, enabled excavation of the fractured substrate, and downslope remobilisation of the megaclasts.

Interbedded heterolithics facies association: description

These deposits are well exposed in measured sections 3, 4 and 6 (**Fig. 2**) where they comprise a series of pebbly sandstones, sandstones, siltstones and shale (**Figs. 7A**, **B**). Beds range from 5- 75 cm in thickness for the sandstones, and 10-50 cm for the siltstones and shale. In vertical section, beds are organised into clear coarsening and thickening upwards (**Figs. 7A, B**) and

315 fining and thinning upwards packages (**Fig. 8C**); a small proportion is ungraded. Individual
316 coarsening-upwards packages reach 20 m thicknesses and can be traced for at least 4 km
317 (**Figs. 1, 2**).

318 The base to all sandstone beds is sharp, and flute casts are locally preserved (**Fig. 7D**).
319 Stacked sandstone beds commonly display a planar, parallel bed top and base (**Fig. 7C**),
320 whereas pebbly sandstone beds resting on siltstones and shales show an irregular to undulose
321 base (**Fig. 7E**, **F**). Structureless and parallel-laminated sandstone beds are common; in places
322 individual beds show a vertical transition from the former to the latter. Current-ripple cross-
323 lamination and small-scale trough cross-bedding (**Fig. 7G**) are developed both toward the top
324 of fining-upward cycles and in ungraded beds. Whereas palaeocurrent data are few, dip-
325 corrected ripple foreset azimuths indicate S to SW palaeoflows. Convolute bedding, ball and
326 pillow structures (**Fig. 7H**) and flame structures are prevalent.

327

328 *Interbedded heterolithics facies association: interpretation*

329 The normally graded sandstone beds record classic T_{abc} turbidites (Talling et al., 2012),
330 consistent with the preservation of flute casts on bed bases, with interbedded siltstone and
331 shale interpreted as the hemipelagic product of waning flow (e.g. Allen et al., 2004). These
332 deposits are considered to be lateral equivalents of the pebble to boulder conglomerate facies
333 association. Downslope evolution of high-density turbidity currents and hyperconcentrated
334 flows results in their dilution as they mix with ambient waters, generating turbulent, lower
335 density flows (Hampton, 1972; Baas et al., 2011; Talling et al., 2012). The generation of
336 these facies via flow transformation of ice-proximal turbidites and debrites is used to argue in
337 favour of a more distal depositional setting, whereas the coarser calibre of the sediment
338 indicates a more proximal setting than comparable low-density turbidites of the lonestone-

bearing facies association. As such, accumulation in the distal reaches of the ice-proximal zone is supported.

Irregular, undulose bed bases indicate cannibalisation of underlying sediments during subsequent turbidity flows, whereas the predominance of planar, non-erosive contacts support hydroplaning during flow emplacement (e.g. Laberg and Vorren, 2000), in a similar manner to the diamictite facies association. This is consistent with the elevated fluid contents anticipated during downslope flow dilution. The presence of convolute lamination and climbing ripple cross-lamination is indicative of rapid deposition under fully turbulent conditions (Allen, 1991; Baas, 2000; Baas et al., 2011; Jobe et al., 2012; Talling et al., 2012). Load and flame structures are indicative of Rayleigh-Taylor instabilities at a grain-size boundary (Allen, 1984).

The stratigraphic arrangement of beds into packages that display clear fining- and coarsening-upwards profiles may imply either autocyclic or allocyclic processes at work. Prélat et al. (2010) recognise a hierarchy of stratigraphic organisation in subaqueous turbidite systems of the Karoo Basin. In descending hierarchical order, lobe complexes are built from lobe elements, in turn built from bedsets and beds. A single subaqueous lobe consists of several vertically stacked lobe elements. The alternation of fine- and coarser-grained packages of multi-metre scale lobe elements in the Kingston Range might thus be suggestive of upstream avulsion of feeder channels (e.g. Prélat et al., 2010). The stratigraphic arrangement of coarsening- and fining-upward cycles (i.e. lobe elements) within this facies association compares closely to similar cycles identified within the pebble to boulder conglomerate facies association (**Fig. 2**, c.f. sections 6 & 7), thus affirming a genetic connection between these deposits.

Evolution of the Kingston Peak Formation

Stacking patterns and inferred glacial cycles

Combining the map distribution of facies associations and their vertical stacking patterns, their 3D distribution can be visualised with the aid of a simple fence diagram (**Fig. 8**). The stratigraphic surface immediately underlying the first occurrence of diamictite (i.e. the KP1-KP2 contact: Prave, 1999) (**Figs. 2, 8**) is a significant unconformity. The overlying diamictite facies association is interpreted as a series of ice-proximal glaciogenic debris flows subject to secondary ice-rafting, and as such represents the onset of glaciation in this region (**Fig. 8**). Arguably, therefore, the basal unconformity which downcuts facies of KP1 may represent a glacial erosion surface (GES). Given the lack of evidence for subglacial features, e.g. ice-contact deformation, within the diamictite facies association, this GES would likely represent subglacial erosion during initial ice advance, which subsequently becomes infilled by glaciogenic debris flows. In this scenario, the erosion surface can be used to support ice grounding in the Kingston Range **(Fig. 9A**). This is a widely recognised unconformity throughout the Death Valley region, defined at the base of the Virgin Spring Limestone due to local angular truncation of the underlying strata (Mrofka, 2010; TU3 of Macdonald et al., 2013). However, this unit is absent throughout the Kingston Range where the unconformity is defined at the base of KP2. Therefore, the region-wide unconformable surface at the top of KP1 clearly has a tectonic origin in places (Macdonald et al. 2013), but is perhaps coincident with a GES in the Kingston Range (sections 1, 2 and 5, **Fig. 2**; **Fig. 9A**).

Macdonald et al. (2013) ascribe the diamictite of KP2 to a single tectonostratigraphic unit. Broadly, the stratigraphic position of that diamictite compares to the stratigraphic position of the diamictite facies association described herein, with one important caveat. We recognise two discrete stratigraphic occurrences of the diamictite facies association, clearly

separated by a lonestone-bearing facies association (which is largely diamictite free) in sections 1, 2 and 5 (**Figs. 2, 8**). We are wary of overemphasising the significance of this interval beyond the Kingston Range, although interestingly Mrofka and Kennedy (2011) also note that the diamictite in KP2 is "interrupted by a 5-20 m interval of finer-grained facies in the Saratoga Hills, southern Saddle Peak Hills and the Alexander Hills". The lonestone-bearing facies association is interpreted to record deposition via dilute turbidity currents and thin glaciogenic debris flows, alongside ice-rafting in interbedded hemipelagic deposits, within an ice-marginal setting (**Fig. 9A**). It therefore reflects a minor retreat phase interrupting ice-proximal deposition of the diamictite facies association, attributed to oscillation of the grounding line as opposed to widespread ice meltback.

The second appearance of ice-proximal diamictites is succeeded by the olistostrome of the megaclast facies association (**Figs. 2, 8**). Release and downslope remobilisation of the megaclasts is attributed to the cumulative effects of syn-sedimentary tectonism, removal of ice cover in the source area and isostatic rebound, triggering ice-berg rafting concomitant with olistolith emplacement. It is therefore interpreted to record an ice minimum phase (**Fig. 9B**). Sufficient meltback to expose bedrock in the source area of the megaclasts, considered to lie a few kilometres north of the outcrop belt (Macdonald et al. 2013), is likely to be more significant than the minor oscillation interrupting accumulation of the diamictite facies association. However, further examination is required to assess the significance of this meltback beyond the Kingston Range, and thus it is important to stress that we do not argue for full interglacial conditions during this interval.

The first stratigraphic appearance of the pebble to boulder conglomerate facies association above the olistostrome complex is abrupt and often sharp-based (**Figs. 2, 8**). These deposits are interpreted to record a sudden influx of coarse debris debouched into the basin during an ice re-advance (**Fig. 9**). The predominance of carbonate boulders derived

412 from the Crystal Spring Formation and Beck Spring Dolomite, i.e. equivalent lithologies to
413 the olistoliths, suggests the exposed bedrock which supplied the megaclasts was equally
414 exploited during the subsequent ice advance. Significant erosion and plucking of the
415 carbonate bedrock would have therefore provided abundant debris for remobilisation as
416 debrites and high-density turbidites of the pebble to boulder conglomerate facies association.
417 The presence of subglacially striated clasts, as reported both by Macdonald et al. (2013) and
418 Mrofka and Kennedy (2011), strongly supports their glacial derivation. The thick,
419 hyperconcentrated deposits are typical of rapid and high rates of sedimentation, commonly
420 encountered within the ice-proximal zone (e.g. Benn and Evans, 2010), corroborated by the
421 preservation of clast striations which would be removed under significant re-working and
422 clast abrasion further downslope.

423 With increasing distance from the ice front, high-density flows of the pebble to
424 boulder conglomerate facies association become diluted, and undergo flow transformation to
425 low-density turbidites and hemipelagic deposits of the interbedded heterolithics facies
426 association. These deposits could be interpreted to record back-stepping of the ice front,
427 thereby preserving a retrogradational sequence of more ice-distal fines overlying ice-
428 proximal conglomerates. However, in places deposits of the interbedded heterolithics and
429 pebble to boulder conglomerate facies associations occur at comparable stratigraphic levels in
430 different logged sections (**Fig. 2**), with no clear upslope to downslope trend (i.e. North to
431 South). This pattern could reflect deposition of the coarser grained facies as turbiditic lobes
432 (sensu Prélat et al., 2009, 2010) with accumulation of finer grained turbidites between coarser
433 lobe elements. The finer grained facies could then be succeeded by the coarser, high-density
434 turbidites (e.g. section 3, **Fig. 2**) under lobe-switching and upstream avulsion. In the Kingston
435 Range, the final deglaciation of the Death Valley region is obscured owing to the angular
436 unconformity that truncates the topmost strata at the base of the Noonday Dolomite.

437

438 *The wider significance of glacial cycles*

439 Based on the stratigraphic organisation of facies associations, we are able to infer advance
440 and retreat of the ice sheets during deposition of the Kingston Peak Formation. The following
441 should be regarded as preliminary, and awaits careful testing in other Death Valley outcrop
442 belts.

443 Evidence of initial ice advance is proposed at the unconformable contact between the
444 pre-glacial KP1 and glacial KP2, interpreted as a glacial erosion surface, at the same
445 stratigraphic level as the more regionally significant tectonic unconformity (base TU3,
446 Macdonald et al., 2013). The first evidence of glacially-influenced sedimentation occurs in
447 the overlying diamictite facies association which records accumulation of glaciogenic debris
448 flows and ice-rafted debris in the ice-proximal zone. A thin interval of ice-marginal turbidites
449 and ice-rafted debris of the lonestone-bearing facies association interrupts this ice-proximal
450 succession, interpreted to record a minor ice front oscillation. Resumed ice-proximal
451 deposition of the diamictite facies association is then succeeded by a more substantial ice
452 meltback during accumulation of the megaclast facies association, wherein ice retreats
453 beyond the source region of the olistoliths in order to enable excavation of the carbonate
454 bedrock. This retreat phase is also associated with disintegration of the ice front, calving ice
455 bergs into the basin which feed debris into the hemipelagic deposits onlapping the olistoliths.
456 A second major ice advance is then recorded in the accumulation of ice-proximal glaciogenic
457 debris flows and turbidites of the pebble to boulder conglomerate facies association, fed by
458 the eroded bedrock which sourced the carbonate megaclasts. Minor back-stepping of the ice
459 front could account for accumulation of more distal low-density turbidites of the interbedded

460 heterolithics facies association towards the top of some logged sections (**Fig. 2**), although
461 evidence of terminal de-glaciation is not recorded.

462 This stratigraphic motif can be used to infer advance and retreat of ice sheets during
463 deposition of the Kingston Peak Formation, although the full extent of ice growth and
464 meltback remains to be tested elsewhere in the Death Valley region, and throughout the
465 Cordillera. The absence of time constraints within the Kingston Peak Formation currently
466 precludes an objective analysis of the cyclicity of these advance-retreat phases. However,
467 recent Re-Os constraints on both the base and top of the Sturtian-equivalent Rapitan
468 succession in NW Canada demonstrate that this glaciation, if global, may have been some 60
469 Ma in duration (Rooney et al., 2013). A ~60 Ma glacial era could clearly incorporate multiple
470 glacial cycles, and multiple glacial events, within the timeframe of a first order global
471 sequence (Catuneanu et al., 2005). Even if we assume that the glacial sedimentary record in
472 the Kingston Range is only a partial record- with cannibalisation of some units demonstrable
473 (**Fig. 9**)- the greatest potential for regional, and global correlation, lies within the thickest
474 accumulations which can be interpreted as major depocentres. Thus, for the purposes of
475 global stratigraphic comparisons with other sections, the Kingston Range is an excellent
476 reference section, even if the significance of the glacial cycles requires further investigation.

477 Classic 'Sturtian' successions in South Australia and northern Namibia both
478 demonstrate evidence for advance and retreat of ice masses during Cryogenian glaciation
479 (e.g. Le Heron et al., 2013; Busfield and Le Heron, 2014), each with an interval of significant
480 ice meltback possibly equating to interglacial conditions. Busfield and Le Heron (2014)
481 propose a high resolution, glacial sequence stratigraphic framework for the central Flinders
482 Ranges in Australia, in which four glacial advance sequences are recognised, separated by
483 three intervals of glacial retreat. One retreat phase also includes evidence of open water
484 conditions, enabling storm-wave agitation of the sediments and generation of hummocky

485 cross-stratification (Le Heron et al., 2011; Busfield and Le Heron, 2014). Sturtian-equivalent
486 deposits of the Chuos Formation in the Omutirapo palaeovalley of northern Namibia likewise
487 preserve evidence of a significant period of ice meltback, wherein a succession of shales
488 lacking glacial influence interrupt the overall ice-proximal regime (Le Heron et al., 2013). It
489 is possible that these intervals of major meltback correlate with the most pronounced retreat
490 in the Kingston Peak succession. However, it is equally plausible that the glacial records are
491 diachronous (e.g. Allen and Etienne, 2008), and hence many more than three glacial cycles
492 can be accommodated within the global 'Sturtian' record. Regardless of which is correct,
493 substantial ice mass wasting and regrowth is necessary to explain the stratigraphy of the
494 Kingston Peak Formation in the Kingston Range. The biggest challenge remains to compare
495 the internal Sturtian record from continent to continent.

496

497 **Conclusions**

498 Based on mapping, sedimentary logging and facies analysis, the Kingston Peak Formation
499 demonstrates a strong glacial influence throughout, subject to advance and retreat of the ice
500 margin. Specific findings are that:-

501 • Five facies associations are recognised in the Kingston Range: 1) diamictite facies
502 association (glacigenic debris flows with secondary ice-berg rafting), 2) lonestone-
503 bearing facies association (hemipelagic deposits and low-density gravity flows with
504 ice-berg rafting), 3) pebble to boulder conglomerate facies association (co-genetic
505 glacigenic debris flows and high-density turbidites), 4) megaclast facies association
506 (olistostrome and hemipelagic sediments subject to ice-rafting), and 5) interbedded
507 heterolithics facies association (low-density turbidites and hemipelagic deposits).

Collectively, these facies testify to the importance of mass flow processes on sedimentation, under an entirely subaqueous regime.

- Deposition of the olistostrome is associated with a period of ice-meltback, enabling exposure of the subglacially fractured carbonate bedrock, and hence release of the olistoliths downslope via removal of the ice buttress, isostatic rebound and syn-sedimentary tectonism.

- The stratigraphic organisation of facies associations enables the glacial history of units KP2 and KP3 of the Kingston Peak Formation to be elucidated, including multiple ice advance-retreat cycles. These are considered to record intra-Sturtian glacial cycles. Overall ice-proximal sedimentation is interrupted by a minor ice front oscillation, and a more significant meltback during deposition of the olistostrome. Terminal de-glaciation is not recorded in the Kingston Range.

This work was supported by a Fermor Fund grant from the Geological Society of London. The authors are very grateful to Francis A. Macdonald, Wolfgang Preiss and Mike Hambrey who provided invaluable, thought provoking suggestions that greatly improved this manuscript. We are also grateful to Phillip Hughes for his editorial work.

References

ABOLINS, M., OSKIN, R., PRAVE, A., SUMMA, C., & CORSETTI, F.A. 2000. Neoproterozoic glacial record in the Death Valley region, California and Nevada (in Great Basin and Sierra Nevada). *Field Guide, Geological Society of America*, **2**, 319–335.

ALLEN, J.R.L. 1984. Sedimentary Structures, their Character and Physical Basis, Unabridged one-volume. Elsevier, Amsterdam, 1256p.

ALLEN, J.R.L. 1991. The Bouma A division and the possible duration of turbidity currents. *Journal of Sedimentary Petrology*, **61**, 291-295.

ALLEN, P.A. & ETIENNE, J.L. 2008. Sedimentary challenge to Snowball Earth. *Nature Geoscience*, **1**, 817-825.

ALLEN, P.A., LEATHER, J., & BRASIER, M.D. 2004. The Neoproterozoic Fiq glaciation and its aftermath, Huqf supergroup of Oman. *Basin Research*, **16**, 507-534.

AMY, L.A. & TALLING, P. 2006. Anatomy of turbidites and linked debrites based on long distance (120 × 30 km) bed correlation, Marnoso Arenacea Formation, Northern Apennines, Italy. *Sedimentology*, **53**, 161–212.

ANDERSON, J.B., KENNEDY, D.S., SMITH, M.J, DOMACK, E.W. 1991. Sedimentary facies associated with Antarctica's floating ice masses. In: *Glacial-marine sedimentation: Paleoclimatic Significance* (Eds J.B. Anderson, G.M. Ashley, G.M), Geological Society of America Special Paper, **261**. Boulder, CO, pp. 1–25.

ARNAUD, E. 2004. Giant cross-beds in the Neoproterozoic Port Askaig Formation, Scotland: implications for snowball Earth. *Sedimentary Geology*, **165**, 155-174.

ARNAUD, E. 2012. The paleoclimatic significance of deformation structures in Neoproterozoic successions. *Sedimentary Geology*, **243-244**, 33-56.

BAAS, J.H. 2000. Duration of deposition from decelerating high-density turbidity currents. *Sedimentary Geology*, **136**, 71-88.

BAAS, J.H., BEST, J.L. & PEAKALL, J. 2011. Depositional processes, bedform development and hybrid flows in rapidly decelerated cohesive (mud-sand) sediment flows. *Sedimentology*, **58**, 1953-1987.

BAGNOLD, R. A. 1954. Experiments on a gravity-free dispersion of large solid spheres in a Newtonian fluid under shear. *Proceedings of the Royal Society of London*, *A*, **225**, 49-63.

BENN, D.I. & EVANS, D.J.A. (Eds.) Glaciers and glaciation. Hodder Education, London, 816 pp.

BUSFIELD, M.E. & LE HERON, D.P. 2013. Glacitectonic deformation in the Chuos Formation of northern Namibia: implications for Neoproterozoic ice dynamics. *Proceedings of the Geologist's Association*. doi: /10.1016/j.pgeola.2012.10.005

BUSFIELD, M.E. & LE HERON, D.P. (2014). Sequencing the Sturtian icehouse: dynamic ice behaviour in South Australia. *Journal of the Geological Society of London*, **124**, 778-789.

CATUNEANU, O., MARTINS-NETO, M.A. & ERIKSSON, P.G. 2005. Precambrian sequence stratigraphy. *Sedimentary Geology*, **176**, 67-95.

CORSETTI, F.A. & KAUFMAN, A.J. 2003. Stratigraphic investigations of carbon isotope anomalies and Neoproterozoic ice ages in Death Valley, California. *Geological Society of America Bulletin*, **115**, 916-932.

568 DIMAKIS, P., ELVERHØI, A., HØEG, K., SOLHEIM, A., HARBLITZ, C., LABERG, S.J.,
569 VORREN, T.O., MARR, J. 2000. Submarine slope stability on highlatitude glaciated
570 Svalbar-Barents Sea margin. *Marine Geology*, **162**, 303-316.

571 DOMACK, E. W., HARRIS, P. 1998. A new depositional model for ice shelves based upon
572 sediment cores recovered in the Ross Sea and Mac.Robertson Shelf, Antarctica. *Annals of*
573 *Glaciology*, **27**, 281-284.

574 DOMACK, E.W. & HOFFMAN, P.F. 2011. An ice grounding-line wedge from the Ghaub
575 glaciation (635 Ma) on the distal foreslope of the Otavi carbonate platform, Namibia, and
576 its bearing on the snowball Earth hypothesis. *Geological Society of America Bulletin*, **123**,
577 1448-1477.

578 DULLER, R., MOUNTNEY, N.P., RUSSELL, A.J. & CASSIDY, N.C. 2008. Architectural analysis
579 of a volcaniclastic jökulhlaup deposit, southern Iceland: sedimentary evidence for
580 supercritical flow. *Sedimentology*, **55**, 939–964.

581 ELVERHØI, A., DE BLASIO, F.V., BUTT, F.A., ISSLER, D., HARBITZ, C.B.,ENGVIK, L., SOLHEIM,
582 A. & MARR, J. 2002. Submarine mass-wasting on glacially influenced continental slopes—
583 processes and dynamics. In: *Glacier-Influenced Sedimentation on High-Latitude*
584 *Continental Margins* (Eds J.A. Dowdeswell and C O'Cofaigh) *Geological Society,*
585 *London, Special Publications*, **203**, 73–87.

586 ETIENNE, P.L., ALLEN, P.A., RIEU, R. & LE GUERROUÉ, E. 2007. Neoproterozoic
587 glaciated basins: a critical review of the Snowball Earth hypothesis by comparison with
588 Phanerozoic glaciations. In: *Glacial Sedimentary Processes and Products* (Eds. M.J.
589 Hambrey, P. Christoffersen, N.F. Glasser & B. Hubbard). Blackwell Publishing Ltd.,
590 Oxford, pp. 343-399.

591 EVANS, J. & PUDSEY, C.J. 2002. Sedimentation associated with Antarctic Peninsula ice
592 shelves: implications for palaeoenvironmental reconstructions of glacimarine sediments.
593 *Journal of the Geological Society of London*, **159**, 233-237.

594 EYLES, N. & JANUSZCZAK, N. 2004. 'Zipper-rift': a tectonic model for Neoproterozoic
595 glaciations during the breakup of Rodinia after 750 Ma. *Earth Science Reviews*, **65**, 1–73.

596 HAMBREY, M. J. & GLASSER, N. F. 2003. GLACIAL SEDIMENTS: PROCESSES, ENVIRONMENTS
597 AND FACIES. IN: MIDDLETON, G.V. (ED.) ENCYCLOPEDIA OF SEDIMENTS AND SEDIMENTARY
598 ROCKS. DORDRECHT: KLUWER, 316-331.

599 HAMBREY, M.J. & GLASSER, N.F. 2012. Discriminating glacier thermal and dynamic regimes
600 in the sedimentary record. *Sedimentary Geology*, **251**, 1-33.

601 HAMPTON, M.A. 1972. The role of subaqueous debris flow in generating turbidity currents.
602 *Journal of Sedimentary Petrology*, 42, 775-793.

603 HAZZARD, J.C. 1939. Possibility of a pre-Cambric glaciation in southeastern California.
604 *Pan-American Geologist*, **71**, 47-48.

HEAMAN, L.M. & GROTZINGER, J.P. 1992. 1.08 Ga diabase sills in the Pahrump Group, California; implications for development of the Cordilleran miogeosyncline. Geology, 20, 637-640.

HECK, F.R. & SPEED, R.C. 1987. Triassic olistostrome and shelf-basin transition in the western Great Basin: Palaeogeographic implications. *Geological Society of America Bulletin*, **99**, 539-551.

HOFFMAN, P.F., KAUFMAN, A.J., HALVERSON, G.P. & SCHRAG, D.P. 1998. A Neoproterozoic Snowball Earth. *Science*, **281**, 1342-1346.

JOBE, Z.R., LOWE, D.R. & MORRIS, W.R. 2012. Climbing-ripple successions in turbidite systems: depositional environments, sedimentation rates and accumulation times. *Sedimentology*, **59**, 867-898.

KENNEDY, M.J., RUNNEGAR, B., PRAVE, A.R., HOFFMANN, K.H., ARTHUR, M.A. 1998. Two of four Neoproterozoic glaciations? *Geology*, **26**, 1059-1063.

KHATWA, A. & TULACZYK, S. 2001. Microstructural interpretations of modern and Pleistocene subglacially deformed sediments: the relative role of parent material and subglacial processes. *Journal of Quaternary Science*, **16**, 507-517.

LABERG, J.S. & VORREN, T.O. 2000. Flow behaviour of the submarine glacigenic debris flows on the Bear Island Trough Mouth Fan, western Barents Sea. *Sedimentology*, **47**, 1105-1117.

LEATHER, J., ALLEN, P.A., BRASIER, M.D., COZZI, A. 2002. Neoproterozoic snowball Earth under scrutiny: Evidence from the Fiq glaciation of Oman. *Geology*, **30**, 891-894.

LE HERON, D.P., BUSFIELD, M.E. & KAMONA, A.F. 2013. Interglacial on snowball Earth? Dynamic ice behaviour revealed in the Chuos Formation, Namibia. *Sedimentology*, **60**, 411-427.

LE HERON, D.P., COX, G.M., TRUNDLEY, A.E., COLLINS, A. 2011. Sea ice-free conditions during the Sturtian glaciation (early Cryogenian), South Australia. *Geology*, **39**, 31–34.

MACDONALD, F.A., PRAVE, A.R., PETTERSON, R., SMITH, E.F., PRUSS, S.B., OATES, K., TROTZUK, D. & FALLICK, A.E. 2013. The Laurentian record of Neoproterozoic glaciation, tectonism, and eukaryotic evolution in Death Valley, California. *Geological Society of America Bulletin*, doi: 10.1130/B30789.1

MARREN, P.M., RUSSELL, A.J. & RUSHMER, E.L. 2009. Sedimentology of a sandur formed by multiple jökulhlaups, Kverkfjöll, Iceland. *Sedimentary Geology*, **213**, 77-88.

MILLER, J.M.G. 1985. Glacial and syntectonic sedimentation: the upper Proterozoic Kingston Peak Formation, southern Panamint Range, California. *Geological Society of America Bulletin*, **96**, 1537-1553.

MILLER, J.M.G. 1987. Paleotectonic and stratigraphic implications of the Kingston Peak-Noonday contact in the Panamint Range, eastern California. *Journal of Geology*, **95**, 75-85.

MONCRIEFF, A.C.M. 1989. Classification of poorly-sorted sedimentary rocks. *Sedimentary Geology*, **65**, 191-194.

MROFKA, D. 2010. *Competing models for the timing of Cryogenian Glaciation: evidence from the Kingston Peak Formation, southeastern California*. PhD dissertation, University of California, Riverside.

MROFKA, D. & KENNEDY, M. 2011. The Kingston Peak Formation in the eastern Death Valley region. In: *The Geological Record of Neoproterozoic Glaciations* (Eds E. Arnaud, G.P. Halverson and G. Shields-Zhou). Geological Society, London, Memoirs, **36**, 449-458.

Ó COFAIGH, C., TAYLOR, J., DOWDESWELL, J.A., ROSELL-MELE, A., KENYON, N.H., EVANS, J. & MIENERT, J. 2002. Sediment reworking on high-latitude continental margins and its implications for palaeoceanographic studies: insights from the Norwegian-Greenland Sea. In: *Glacier-Influenced Sedimentation on High-Latitude Continental Margins* (Eds J.A. Dowdeswell, J.A. and C Ó'Cofaigh) *Geological Society, London, Special Publications*, **203**, 325–348.

PETTERSON, R., PRAVE, A.R., WERNICKE, B.P. & FALLICK, A.E. 2011a. The Neoproterozoic Noonday Formation, Death Valley region, California. *Geological Society of America Bulletin*, **123**, 1317-1336.

PETTERSON, R., PRAVE, A.R. & WERNICKE, B.P. 2011b. Glaciogenic and related strata of the Neoproterozoic Kingston Peak Formation in the Panamint Range, Death Valley region, California. In: *The Geological Record of Neoproterozoic Glaciations* (Eds E. Arnaud, G.P. Halverson and G. Shields-Zhou). Geological Society, London, Memoirs, **36**, 449-458.

PHILLIPS, E. 2006. Micromorphology of a debris flow deposit: evidence of basal shearing, hydrofacturing, liquefaction and rotational deformation during emplacement. *Quaternary Science Reviews*, **25**, 720-738.

PRAVE, A.R. 1999. Two diamictites, two cap carbonates, two $\delta^{13}C$ excursions, two rifts: the Neoproterozoic Kingston Peak Formation, Death Valley, California. *Geology*, **27**, 339-324.

PRELAT, A., HODGSON, D.M. & FLINT, S.S. 2009. Evolution, architecture and hierarchy of distributary deep-water deposits: a high-resolution outcrop investigation from the Permian Karoo Basin, South Africa. *Sedimentology*, **56**, 2132-2154.

PRÉLAT, A., COVAULT, J.A., HODGSON, D.M., FILDANI, A. & FLINT, S.S. 2010. Intrinsic controls on the range of volumes, morphologies, and dimensions of submarine lobes. *Sedimentary Geology*, **232**, 66-76.

PUDSEY, C. J., MURRAY, J. W., APPLEBY, P. & EVANS, J. 2006. Ice shelf history from petrographic and foraminiferal evidence, northeast Antarctic Peninsula. *Quaternary Science Reviews*, **25**, 2357–2379.

REINARDY, B. T. I., PUDSEY, C. J., HILLENBRAND, C.-D., MURRAY, T. & EVANS, J. 2009. Contrasting sources for glacial and interglacial shelf sediments used to interpret changing ice-flow directions in the Larsen Basin, northern Antarctic Peninsula. *Marine Geology*, **266**, 156-171.

ROBERTSON, A.H.F. 1977. The Moni Mélange, Cyprus: an olistostrome formed at a destructive plate margin. *Journal of the Geological Society, London*, **133**, 447-466.

ROONEY, A.D., MACDONALD, F.A., STRAUSS, J.V., DUDÁS, F. Ö., HALLMANN, C. AND SELBY, D. 2013. Re-Os geochronology and coupled Os-Sr isotope constraints on the Sturtian snowball Earth. *Proceedings of the National Academy of Sciences*, **111**, 51-56.

SHELDON, N.D. & TABOR, N.J. 2009. Paleoenvironmental and paleoclimatic reconstruction using paleosols. *Earth-Science Reviews*, **95**, 1-52.

TALLING, P.J., MASSON, D.G., SUMNER, E.J. & MALGESINI, G. 2012. Subaqueous sediment density flows: depositional processes and deposit types. *Sedimentology*, **59**, 1937-2003.

TINTERRI R., DRAGO, M., CONSONNI, A., DAVOLI, G. & MUTTI, E. 2003. Modelling subaqueous bipartite sediment gravity flows on the basis of outcrop constraints: first results. *Marine and Petroleum Geology*, **20**, 911-933.

TROXEL, B.W. 1966. Sedimentary features of the Later Precambrian Kingston Peak Formation, Death Valley, California. *Geological Society of America Special Paper*, **101**, 341p.

TROXEL, B.W. 1982. Description of the uppermost part of the Kingston Peak Formation, Amargosa Rim canyon, Death Valley region, California. In: *Geology of selected areas in the San Bernadino Mountains, western Mojave Desert, and southern Great Basin, California* (Eds J.D. Cooper, B.W. Troxel, L.A. Wright), Geological Society of America (Cordilleran Section) volume and guidebook. Shoshone, CA, Death Valley Publishing Company, 61-70.

VORREN, T.O., BLAUME, F., DOWDESWELL, J.A., LABERG, J.S., MIENERT, J., RUMOHR, J. & WERNER, F. 1998. The Norwegian-Greenland Sea continental margins: morphology and late Quaternary sedimentary processes and environments. *Quaternary Science Reviews*, **17**, 273-302.

WENDORFF, M. 2005. Lithostratigraphy of Neoproterozoic syn-rift sedimentary megabreccia from Mwambashi, Copperbelt of Zambia, and correlation with olistostrome succession from Mufulira. *South African Journal of Geology*, **108**, 505-524.

WRIGHT, L.A., TROXEL, B.W., WILLIAMS, E.G., ROBERTS, M.T. & DIEHL, P.E. 1974. Precambrian Sedimentary Environments of the Death Valley Region, Eastern California. In: *Guidebook: Death Valley region, California and Nevada* (Eds B.W. Troxel, L.A. Wright, L.A). Death Valley Publishing Company, Shoshone, CA., 27-35.

Figure captions

Figure 1. Geological map of the NE Kingston Range, compiled from field observations in concert with satellite image interpretation. Distribution of the olistoliths in the vicinity of section 5 is after Macdonald et al. (2013). The map shows the distribution of those facies associations described and interpreted in this paper. Stratigraphic dips of the Beck Spring Dolomite and the overlying Kingston Peak Formation fan around the periphery of the granite intrusion that dominates the range. Note substantial lateral thickness variations of the Kingston Peak Formation, with a general increase toward the SE. This trend is interrupted by a comparatively reduced thickness in the vicinity of the Horsethief Spring (section 3), where en echelon faults transecting the succession can be clearly observed. Inset map shows the location of the Kingston Range in its regional context.

Figure 2. Correlation panel for seven detailed sections (locations shown on Fig. 1). This NW-SE traverse is hung from the Noonday Dolomite as a datum. The top of measured section 5 is at least 1 km stratigraphically below the Noonday Dolomite (see Fig. 1) and thus the total thickness of the Kingston Peak Formation is at least 1200 m in this part of the range. The apparent continuity of the lonestone-bearing facies association is arrested by truncation beneath a thick accumulation of boulder conglomerates (section two). Co-ordinates of sections are as follows. (1) 35°47.924'N 115°57.773'W (base), 35°48.074'N 115°57.673'W (top & Noonday contact); (2) 35°47.795'N 115°55.628'W (base Kingston

738 Peak Fm), 35°48.253'N 115°55.635'W (top: base of Noonday); (3) 35°46.201'N
739 115°52.577'W (base), 35°46.315'N 115°52.207'W (top); (4) 35°45.489'N 115°50.603'W
740 (base), 35°45.528'N 115°50.497'W (top) (5) 35°44.810'N 115°51.612'W (base of
741 diamictite), 35°44.843'N 115°51.137'W (top of olistolith) (6) 35°45.282'N 115°50.053'W
742 (top), 35°45.235'N 115°50.167'W (base); (7) 35°44.034'N 115°49.325'W (base & contact
743 with olistolith), 35°44.291'N 115°49.057'W (top & Noonday contact).

744 *Figure 3*: Aspects of the diamictite facies association. A: Interbedded carbonate-rich and
745 siliciclastic-rich diamictites on the multi-metre scale (section 1, 60-65 m, Fig. 3). B: Typical
746 example of a striated cobble from the Kingston Peak Formation, collected from ca. 40 m
747 from the base of section 1. Striated clasts are very common, and were recovered from each
748 studied outcrop of this facies association. C: Stratified diamictite with 2 cm diameter
749 lonestones (section 5, 45 m, Fig. 3). D: Stratified diamictite composed of highly attenuated
750 laminae in the brown strata and showing intercalations of granular and clast-free siltstone
751 horizons on the cm-scale (section 5, 46 m, Fig. 3). E: Fresh face of massive diamictites
752 (section 3, 90 m, Fig. 3). F: Thin section micromorphology of the stratified diamictite facies
753 (section 5, 48 m, Fig. 3).

754 *Figure 4*: Aspects of the lonestone-bearing facies association. A: Typical example of a
755 ferruginous facies, with well stratified siltstones and well expressed bedding. Pebble trains,
756 defining some of the bed bases, are arrowed. B: Boulder-sized, buff coloured dolostone
757 clast- an isolated lonestone, without associated pebble train. C: A lonestone downwarping
758 and piercing siltstone laminae beneath it. Note that overlying laminae are undeformed. All
759 examples from section 5, ca. 105 m from base: see Fig. 3.

760

761 *Figure 5*: Boulder conglomerate facies association. A: Boulder conglomerate (110 m on
762 section 3: see Fig. 3 for stratigraphic position). B: Fining upward motif (approximately
763 delineated by hammer), with an overlying coarsening upward motif. C: Decimetre-scale
764 trough cross-strata downlapping onto differentially silicified sandstones. D: Dramatic vertical
765 facies shift from conglomerate beds to overlying black, silicified shales and sandstones (113-
766 115 m, section 6).

767

768 *Figure 6*: Megaclast facies association. A: Photo taken looking north whilst completing log
769 5, and taken from the top of an olistolith (in foreground, and at 140 m on log: see Fig. 3).
770 Field of view is approximately 3 km in midground. B: Line drawing over photo of A,
771 illustrating the geometry of the olistoliths, their blocky character at the kilometre-scale, the
772 outcrop width of the olistostrome in general, and the disconnected Noonday Dolomite peaks
773 capping the Kingston Peak Formation in the distance. Note also the shale beds onlapping the
774 cliff-forming olistolith in the middle of the photograph. C: Blocky, angular carbonate boulder
775 of the Beck Spring Dolomite (226 m on log 2: see Fig. 3), encased within red siltstone. These
776 deposits are interpreted as lateral equivalents of the olistostrome shown in A and B. D:
777 Carbonate-rich diamictite, with highly attenuated clasts of Crystal Spring Formation
778 stromatolite.. The diamictite is well stratified, with the fabric dipping steeply toward the left
779 of the photograph. E: Arkose megaclast, with hammer for scale. F: Onlap of shale against
780 olistolith. The photo is an area of detail shown in A and B..

781

782 *Figure 7*: Interbedded heterolithics facies association. A: Coarsening up shales and siltstones
783 to the left of the hammer (circled) and thickening up sandstones and conglomerates (right of
784 the hammer). B: Detail of A, with thick sandstone bed clearly showing truncation of

785 underlying strata. C: Stacked fining upward successions developed in a sandstone package.
786 D: Flute casts at the base of a bed. Palaeocurrent was moving toward 030°. E: Normal
787 grading: fining up from a granular conglomerate at the base of the lens cap to medium-
788 grained sandstone at the top of the bed. F: Granular conglomerate, with an undulose base,
789 cutting into siltstone. G: Trough-cross stratification in coarse-grained sandstone. H:
790 Interlaminated siltstone (dark grey) and shale (light grey / brown) with low amplitude load
791 structures in the lamina beneath the coin. Photos A, B, E, F, G, H from section 6 (60-110 m);
792 photo D from section 3 (145 m); photo C from section 4 (105-110 m).

793 *Figure 8*. Fence diagram based on Fig. 3, attempting to show the 3D organisation of facies
794 association based on the relative map positions of the correlated sections as shown in Fig. 1.

795 *Figure 9*: Sequence of models illustrating the evolution of the Kingston Peak Formation in
796 the context of glacial cycles in the Kingston Range.

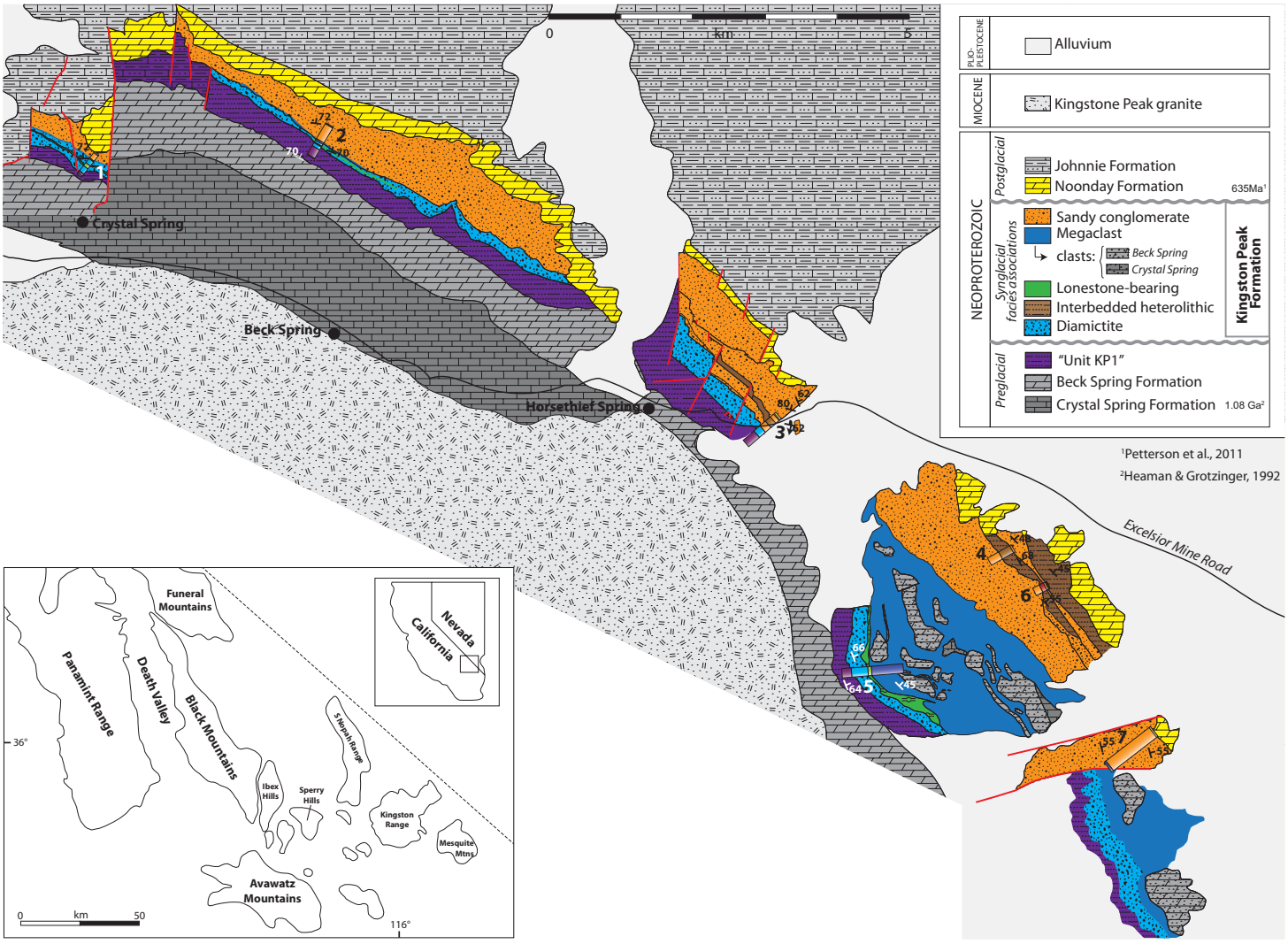
0
km
5
Crystal Spring
Beck Spring
Horsethief Spring
Excelsior Mine Road
PLIO-PLEISTOCENE
Alluvium
MIOCENE
Kingstone Peak granite
NEOPROTEROZOIC
Postglacial
Johnnie Formation
Noonday Formation
635Ma[1]
Synglacial facies associations
Sandy conglomerate
Megaclast
clasts:
Beck Spring
Crystal Spring
Lonestone-bearing
Interbedded heterolithic
Diamictite
Kingston Peak Formation
Preglacial
"Unit KP1"
Beck Spring Formation
Crystal Spring Formation
1.08 Ga[2]
[1]Petterson et al., 2011
[2]Heaman & Grotzinger, 1992
Funeral Mountains
Panamint Range
Death Valley
Black Mountains
Ibex Hills
Sperry Hills
Kingston Range
Mesquite Mtns
Avawatz Mountains
Nevada
California
36°
116°
0
km
50

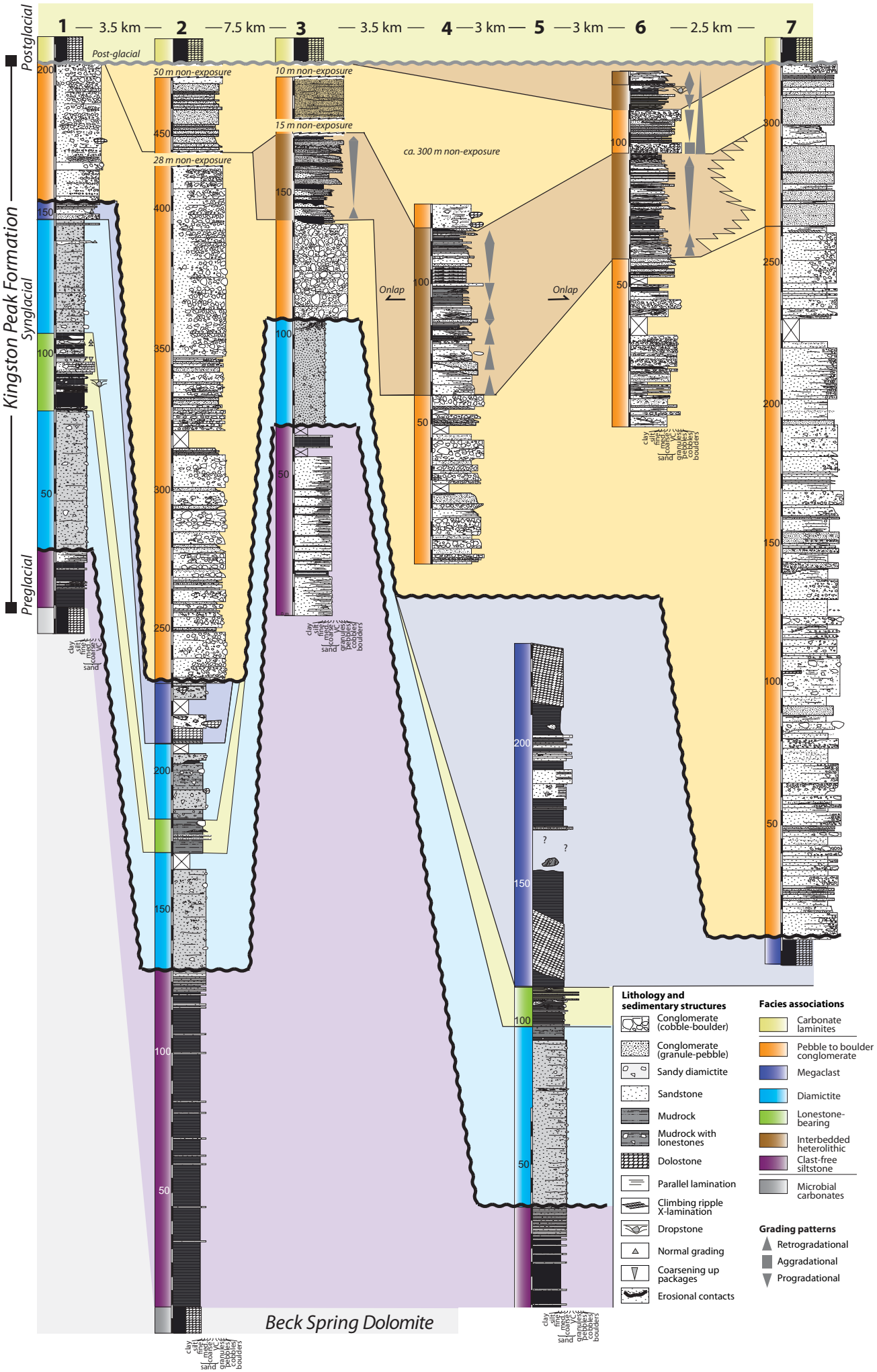
1
3.5 km
2
7.5 km
3
3.5 km
4
3 km
5
3 km
6
2.5 km
7
Postglacial
Kingston Peak Formation
Synglacial
Preglacial
Post-glacial
50 m non-exposure
28 m non-exposure
10 m non-exposure
15 m non-exposure
ca. 300 m non-exposure
Onlap
Onlap
Beck Spring Dolomite
clay
silt
mud
fine
med
coarse
VC
sand
granules
pebbles
cobbles
boulders
Lithology and sedimentary structures
Conglomerate (cobble-boulder)
Conglomerate (granule-pebble)
Sandy diamictite
Sandstone
Mudrock
Mudrock with lonestones
Dolostone
Parallel lamination
Climbing ripple X-lamination
Dropstone
Normal grading
Coarsening up packages
Erosional contacts
Facies associations
Carbonate laminites
Pebble to boulder conglomerate
Megaclast
Diamictite
Lonestone-bearing
Interbedded heterolithic
Clast-free siltstone
Microbial carbonates
Grading patterns
Retrogradational
Aggradational
Progradational

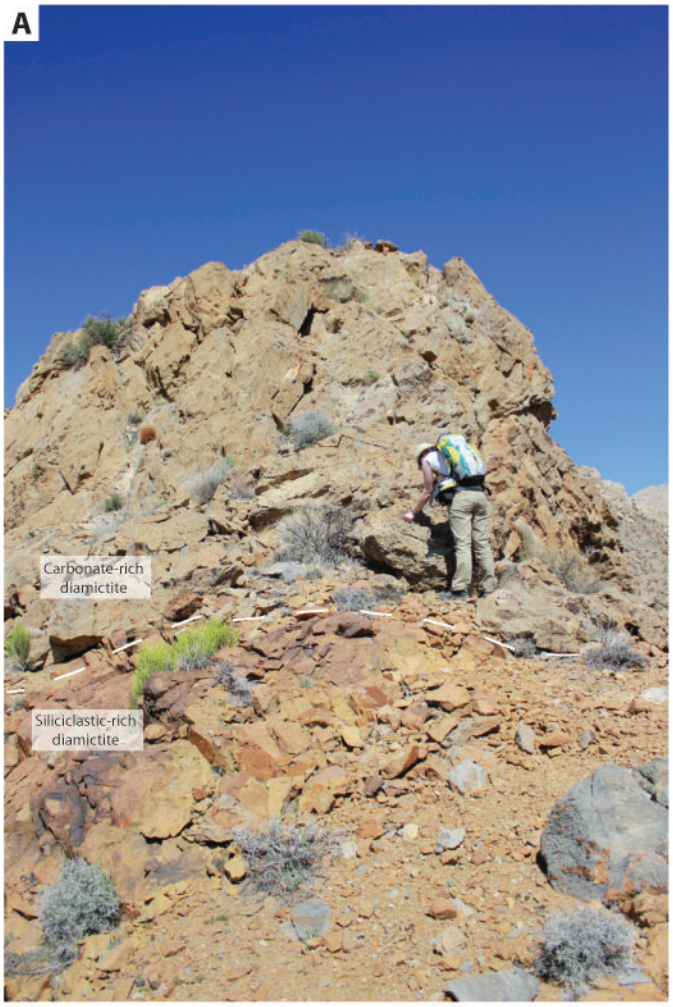
A
Carbonate-rich diamictite
Siliciclastic-rich diamictite


B


C

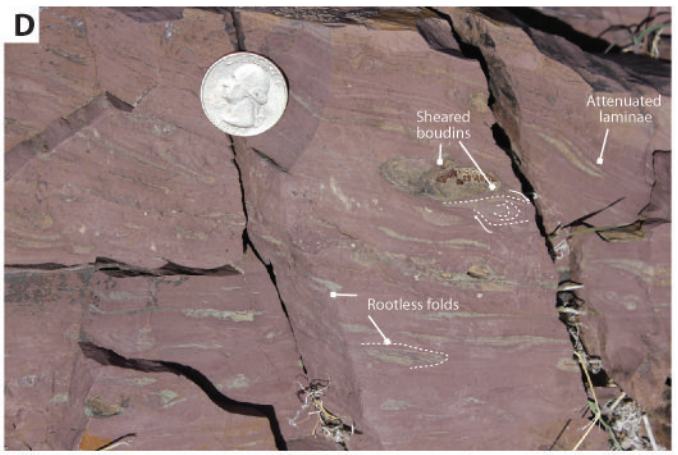
D
Sheared boudins
Attenuated laminae
Rootless folds


E

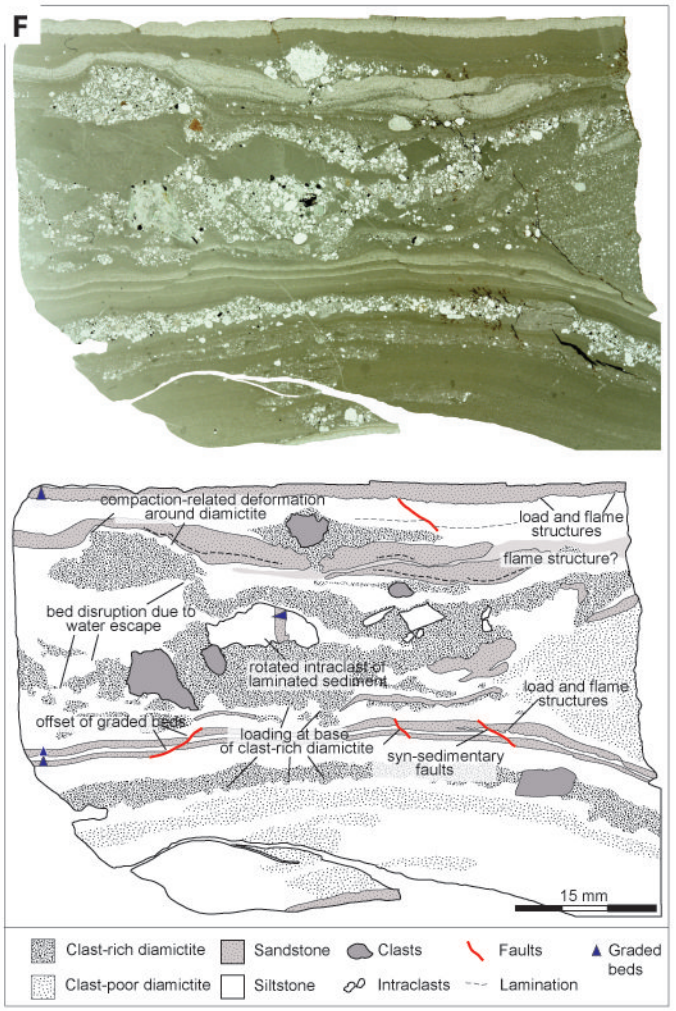
F
compaction-related deformation around diamictite
load and flame structures
flame structure?
bed disruption due to water escape
rotated intraclast of laminated sediment
load and flame structures
offset of graded beds
loading at base of clast-rich diamictite
syn-sedimentary faults
15 mm
Clast-rich diamictite
Clast-poor diamictite
Sandstone
Siltstone
Clasts
Intraclasts
Faults
Lamination
Graded beds

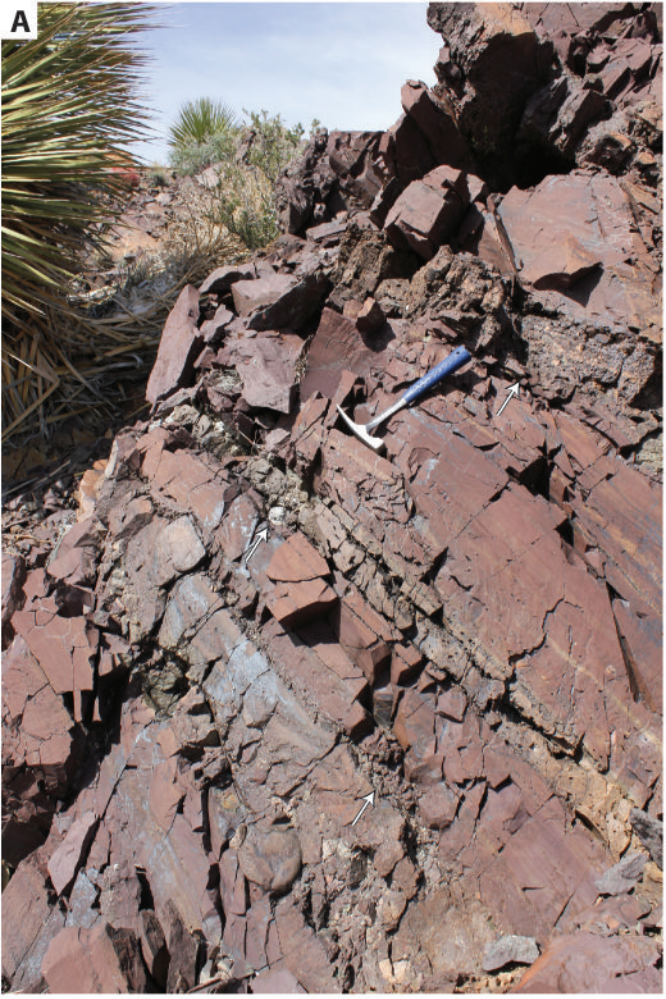
A

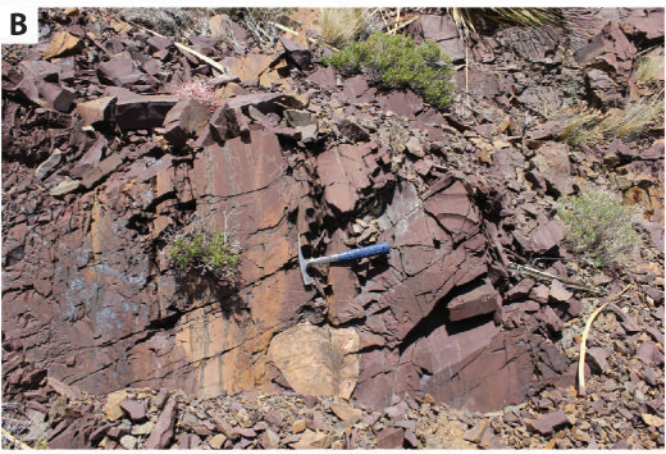
B

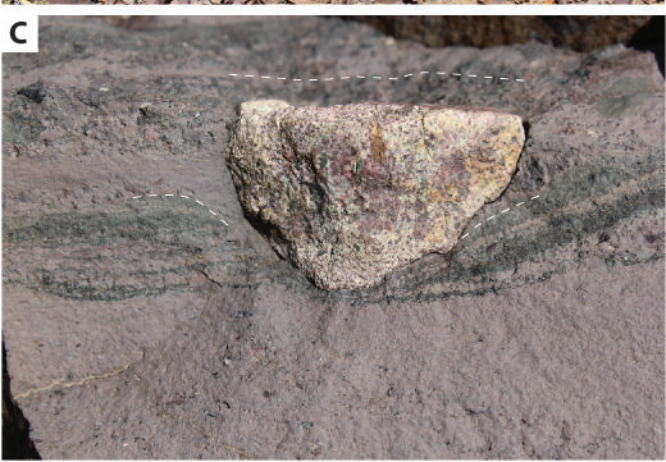
C

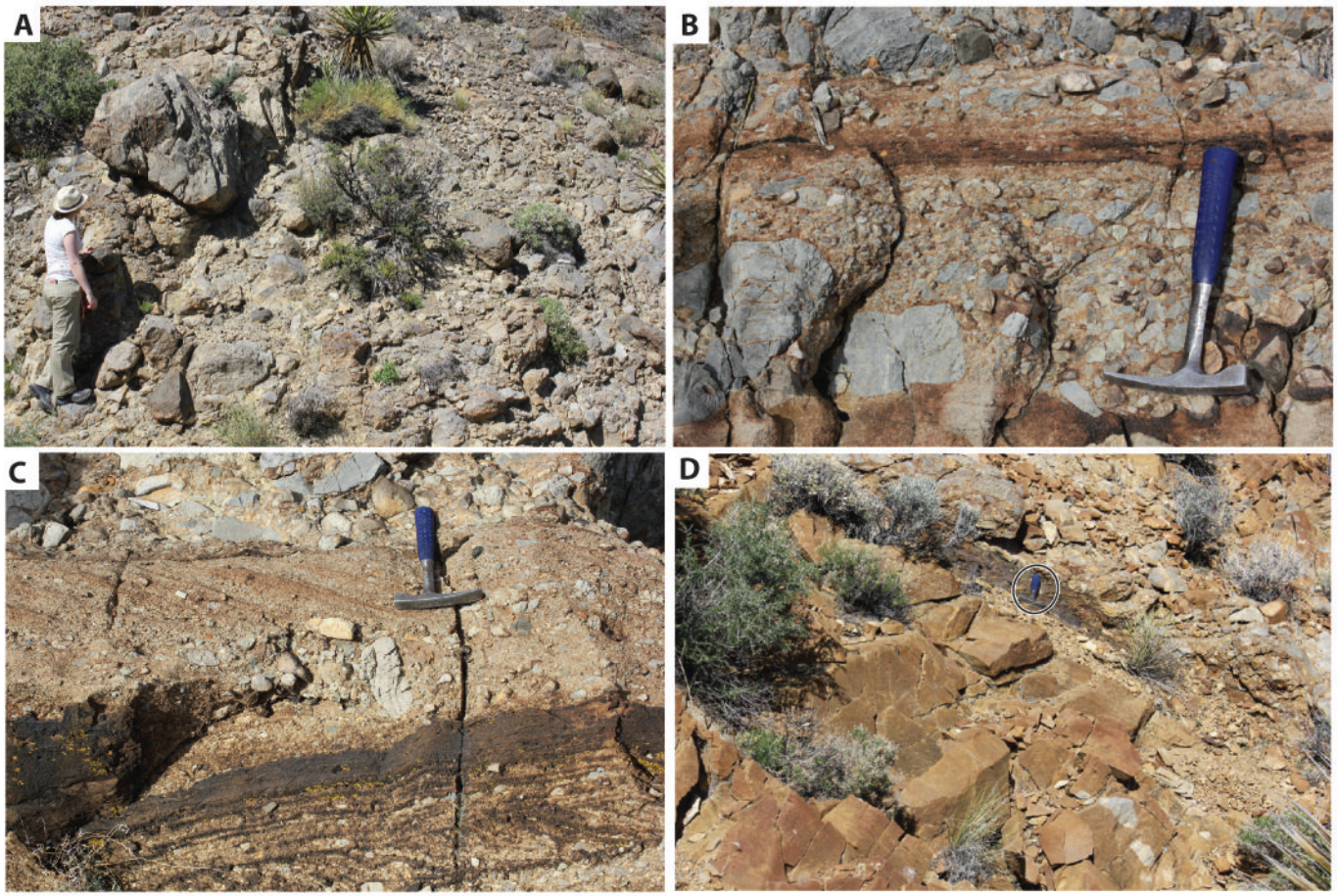
A
B
C
D

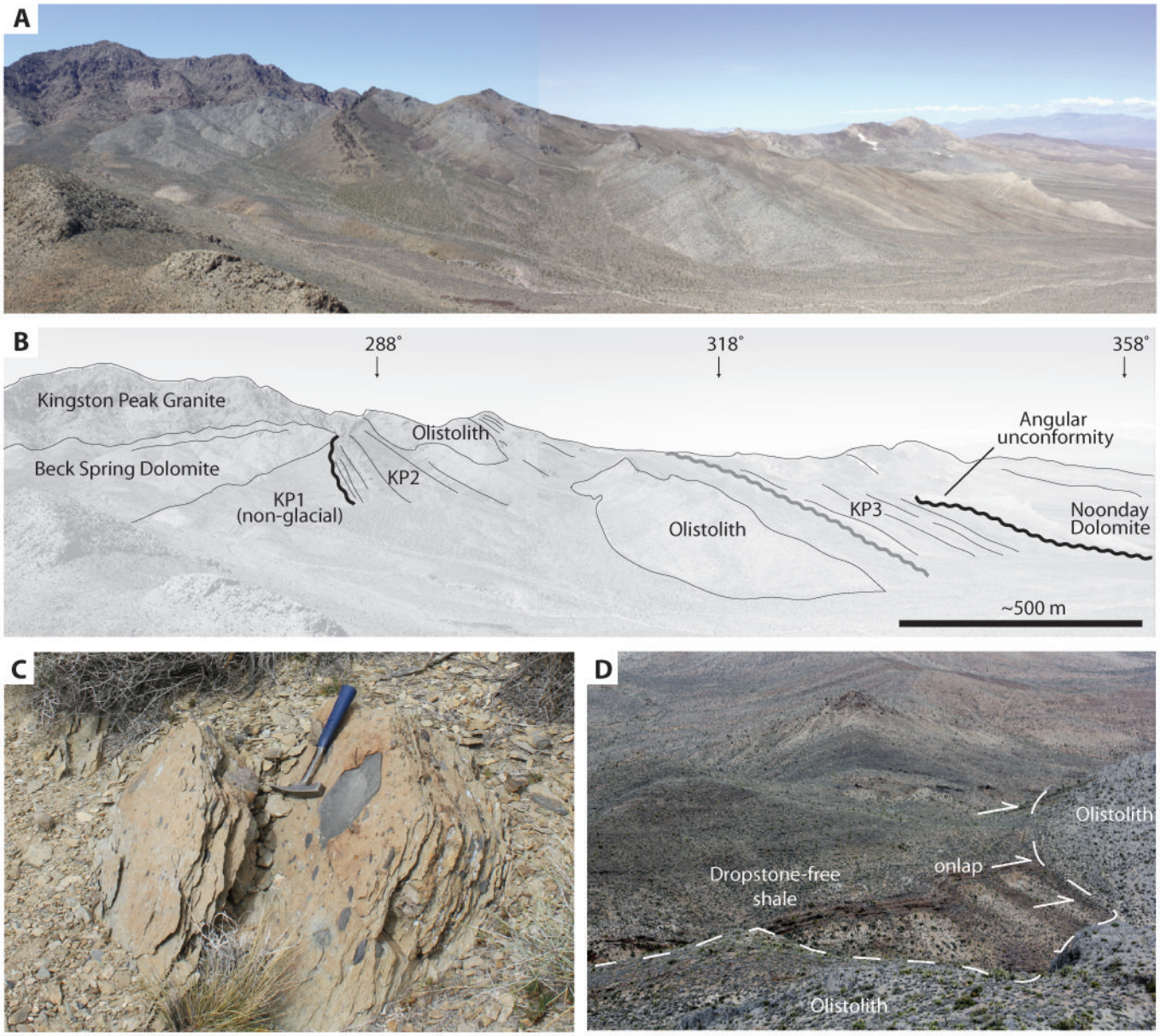
A
B
288°
318°
358°
Kingston Peak Granite
Beck Spring Dolomite
KP1
(non-glacial)
Olistolith
KP2
Olistolith
KP3
Angular
unconformity
Noonday
Dolomite
~500 m
C
D
Olistolith
onlap
Dropstone-free
shale
Olistolith

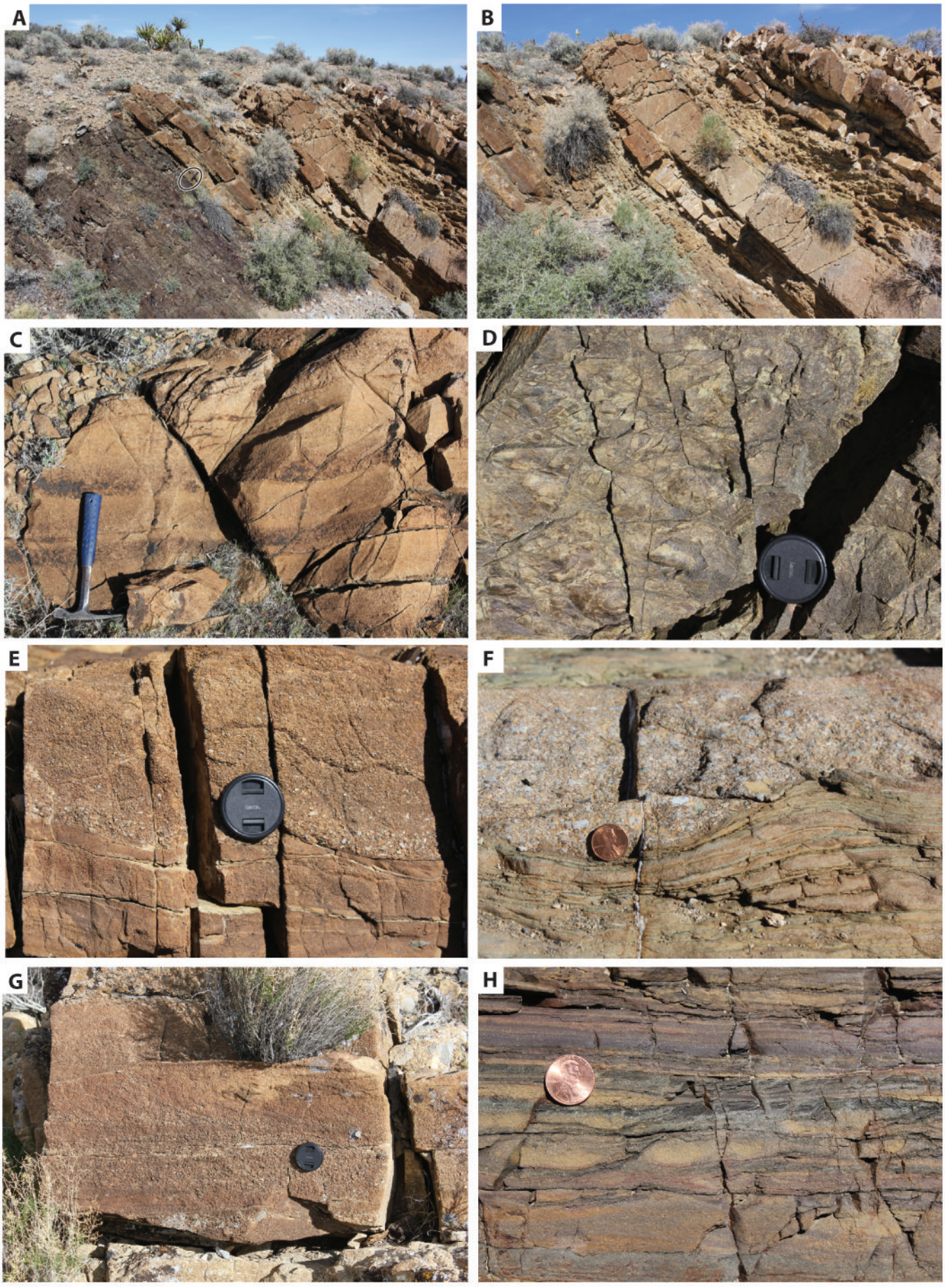
A
B
C
D
E
F
G
H

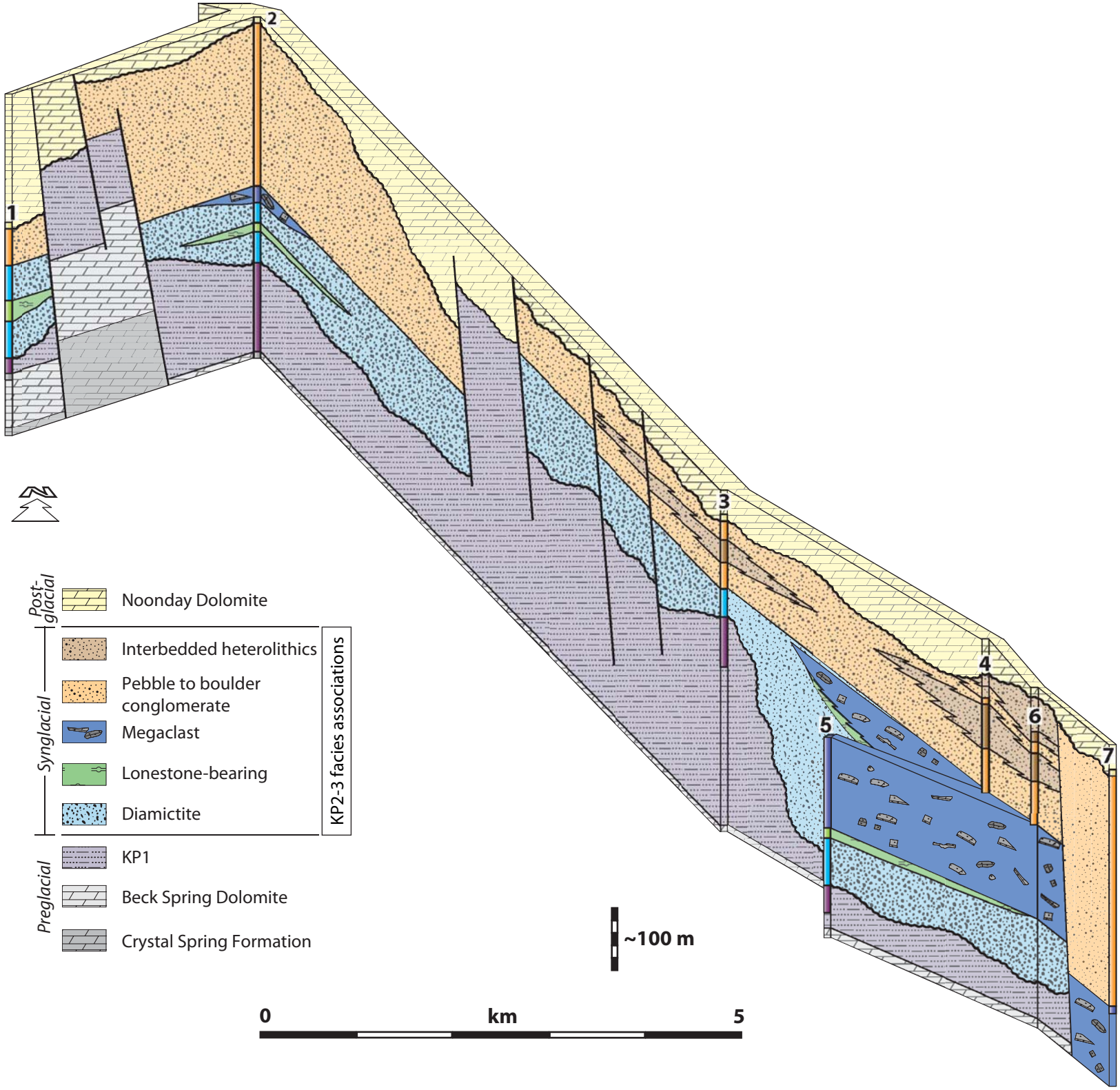
1
2
3
4
5
6
7
Post-glacial
Noonday Dolomite
Synglacial
Interbedded heterolithics
Pebble to boulder conglomerate
Megaclast
Lonestone-bearing
Diamictite
KP2-3 facies associations
Preglacial
KP1
Beck Spring Dolomite
Crystal Spring Formation
~100 m
0
km
5

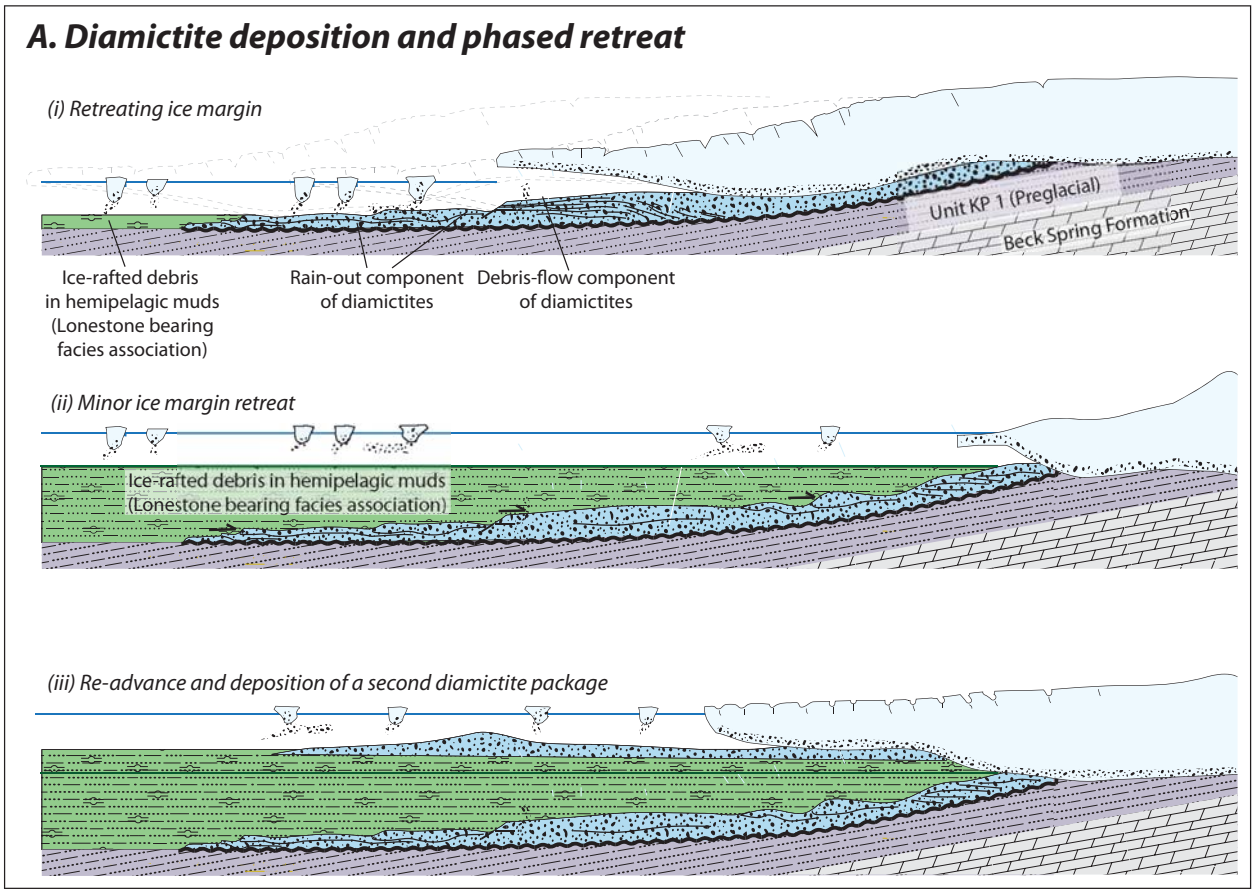
A. Diamictite deposition and phased retreat
(i) Retreating ice margin
Unit KP 1 (Preglacial)
Beck Spring Formation
Ice-rafted debris in hemipelagic muds (Lonestone bearing facies association)
Rain-out component of diamictites
Debris-flow component of diamictites
(ii) Minor ice margin retreat
Ice-rafted debris in hemipelagic muds (Lonestone bearing facies association)
(iii) Re-advance and deposition of a second diamictite package
B. Emplacement of olistostrome
(iv) Possible isostatic rebound of hinterland
Olistoliths
Carbonate exposure/ unroofing
Megaclast facies association
Xtal Spring Fm
C. Glacial re-advance
(v) Erosion of carbonate hinterland at glacial maximum
Turbidites
Non-cohesive debris flows
Interbedded heterolithics
Sandy Conglomerate facies association